



U.S. Department  
of Transportation

**National Highway  
Traffic Safety  
Administration**



---

DOT HS 812 249

March 2016

# **Determination of Battery Stability With Advanced Diagnostics**

## Disclaimer

This publication is distributed by the U.S. Department of Transportation, National Highway Traffic Safety Administration, in the interest of information exchange. The opinions, findings, and conclusions expressed in this publication are those of the authors and not necessarily those of the Department of Transportation or the National Highway Traffic Safety Administration. The United States Government assumes no liability for its contents or use thereof. If trade or manufacturers' names or products are mentioned, it is because they are considered essential to the object of the publication and should not be construed as an endorsement. The United States Government does not endorse products or manufacturers.

Suggested APA Format Citation:

Lamb, J., Orendorff, C. J., & Christophersen, J. P. (2016, March). *Determination of battery stability with advanced diagnostics* (Report No. DOT HS 812 249). Washington, DC: National Highway Traffic Safety Administration.

**Technical Report Documentation Page**

|   |  |   |  |   |  |
|---|--|---|--|---|--|
| 1. Report No.<br><b>DOT HS 812 249</b>  |  | 2. Government Accession No.                                 |  | 3. Recipients's Catalog No.   |  |
| 4. Title and Subtitle<br><b>Determination of Battery Stability with Advanced Diagnostics</b>  |  |   |  | 5. Report Date<br><b>March 2016</b>   |  |
|   |  |   |  | 6. Performing Organization Code   |  |
| 7. Authors<br><b>Joshua Lamb and Christopher J. Orendorff, Advanced Power Sources R&amp;D, Sandia National Laboratories, Albuquerque, NM, and Jon P. Christophersen, Energy Storage and Transportation Systems Department, Idaho National Laboratory, Idaho Falls, ID</b>   |  |   |  | 8. Performing Organization Report No.   |  |
| 9. Performing Organization Name and Address<br><b>Sandia National Laboratory<br/>Albuquerque, New Mexico 87185</b>  |  |   |  | 10. Work Unit No. (TRAI)n code  |  |
|   |  |   |  | 11. Contract of Grant No.<br><b>DTNH22-14-X-00453-0</b>   |  |
| 12. Sponsoring Agency Name and Address<br><b>National Highway Traffic Safety Administration<br/>1200 New Jersey Ave, S.E.<br/>Washington, DC 20590</b>  |  |   |  | 13. Type of Report and Period Covered<br><b>Interim milestone report 8/14-12/14</b>   |  |
|   |  |   |  | 14. Sponsoring Agency Code  |  |
| 15. Supplementary Notes   |  |   |  |   |  |
| 16. Abstract<br><p>The increasing demand for lithium ion batteries for vehicle electrification is changing the typical-use conditions that batteries may see. Over time batteries may develop defects that are difficult to detect with traditional measurements. It is also possible that batteries may be left in an unknown state after failure of the monitoring system, loss of communication, or a potentially damaging event such as a car crash. It is therefore useful to explore other monitoring and interrogation methods that can better determine the stability of a battery in an unknown state. This work explores the use of electrochemical impedance spectroscopy as a method to determine the stability of batteries by observing changes in the complex impedance measurement as the cell is exposed to abusive conditions. Very dramatic changes to the internal resistance were observed when single cells were exposed to abusive conditions, suggesting that even single frequency impedance measurements could be effective with single cells. However, tests on three-cell series and parallel strings yielded smaller changes, primarily to the charge transfer resistance, showing that complex impedance measurements are more appropriate as the system increases in complexity. A rapid-impedance tool developed at Idaho National Laboratory was tested and compared to traditional potentiostat tools as well. This tool was shown to yield similar data to the traditional tools, providing a potential method for continuous monitoring of a battery system. It was observed, however, that shifts in data are difficult to detect in very transient systems.</p> |  |   |  |   |  |
| 17. Key Words<br><b>lithium ion, Li-ion, batteries</b>  |  |   |  | 18. Distribution Statement<br><b>Document is available to the public from the National Technical Information Service<br/><a href="http://www.ntis.gov">www.ntis.gov</a></b> |  |
| 19. Security Classif. (of this report)<br><b>Unclassified</b>   |  | 20. Security Classif. (of this page)<br><b>Unclassified</b> |  | 21. No of Pages<br><b>42</b>  |  |
|   |  |   |  | 22. Price   |  |

**DOT F1700.7 (8-72)** Reproduction of completed page authorized

## **ACKNOWLEDGMENTS**

This work was funded by the Department of Transportation's National Highway Traffic Safety Administration. We would like to thank our project sponsors Phillip Gorney and Stephen Summers.

Sandia National Laboratories is a multi-program laboratory managed and operated by Sandia Corporation, a wholly owned subsidiary of Lockheed Martin Corporation, for the U.S. Department of Energy's National Nuclear Security Administration under contract DE-AC04-94AL85000.

This work was prepared as an account of work sponsored by an agency of the United States Government under INL Contract # DE-AC07-05ID14517.

# CONTENTS

|   |    |
|---|----|
| 1. Introduction.....  | 1  |
| 1.1. Stability of abused batteries .....                        | 1  |
| 1.2. Electrochemical impedance spectroscopy .....               | 5  |
| 1.3. Rapid-impedance measurement tools .....                    | 6  |
| 2. Experimental methods .....                                   | 9  |
| 2.1 Single-cell testing.....                                    | 9  |
| 2.1.1 Single-cell overcharge testing .....                      | 9  |
| 2.1.2 Single-cell thermal ramp testing.....                     | 9  |
| 2.2 Three-cell string testing .....                             | 9  |
| 2.2.1 Series testing (3S1P) .....                               | 10 |
| 2.2.2 Parallel-string testing (1S3P).....                       | 10 |
| 2.3 Testing with the INL rapid-impedance measurement tool ..... | 10 |
| 3. Results.....   | 12 |
| 3.1 Cell selection, validation and initial testing .....        | 12 |
| 3.2 Single-cell overcharge testing.....                         | 15 |
| 3.3 Single-cell thermal ramp testing .....                      | 18 |
| 3.4 Three-cell string overcharge testing.....                   | 19 |
| 3.5 Three-cell string thermal ramp testing.....                 | 20 |
| 3.6 Evaluation of INL rapid-impedance measurement tool.....     | 23 |
| 4. Conclusions.....   | 29 |
| 4.1 Technical challenges and future directions.....             | 30 |
| 5. References.....  | 32 |

## FIGURES

|           |   |    |
|-----------|---|----|
| Figure 1  | Cell voltage and skin temperature as a function of state-of-charge during a 2C overcharge test of a 12 Ah lithium-ion cell. ....  | 3  |
| Figure 2  | Cell voltage and skin temperature as a function of time during a blunt-nail penetration test of a 2 Ah 18650 cell.....  | 4  |
| Figure 3  | Cell self-heating rate ( $^{\circ}\text{C}/\text{min}$ ) as a function of temperature of a 2 Ah 18650 cell during a thermal ramp test at ramp rate of $5^{\circ}\text{C}/\text{min}$ .....  | 4  |
| Figure 4  | Impedance spectrum Nyquist curve [22].....  | 6  |
| Figure 5  | Generation 1 IMB.....   | 7  |
| Figure 6  | Generation 3 IMB attached to a 12 V lead-acid module.....   | 7  |
| Figure 7  | Voltage and current during 1C rate (10 A) overcharge of 10 Ah prismatic pouch cell. Cell failure can be seen at $\sim 198\%$ SOC.....   | 12 |
| Figure 8  | Cell temperatures during 1C rate (10A) overcharge of 10 Ah prismatic pouch cell. Maximum temperatures during cell failure were observed as high as $1113^{\circ}\text{C}$ . ....  | 13 |
| Figure 9  | Cell temperatures and voltage during thermal ramp test of 10 Ah prismatic pouch cell. Onset of thermal runaway occurred at $\sim 171^{\circ}\text{C}$ with observed temperatures up to $617^{\circ}\text{C}$ . ....   | 14 |
| Figure 10 | Validation testing of INL impedance measurement hardware showing EIS data for a commercial 18650 cell. ....   | 14 |
| Figure 11 | Validation testing of INL impedance measurement hardware showing little drift in EIS data collected over 10 separate measurements of a cell under the same experimental conditions. ....  | 15 |
| Figure 12 | Impedance data collected from 100% to 200% SOC prior to cell failure.....   | 16 |
| Figure 13 | Temperature data as a function of total state of charge. The cooling observed at $\sim 180\%$ and $\sim 200\%$ was due to cooling that occurred during the halt of overcharge testing. The dashed arrows show the corresponding points of data collection. ....   | 17 |
| Figure 14 | Impedance data of two overcharge tests showing potential repeatability of measurements. While the general behavior of the two tests is very similar a shift of $\sim 8\text{ m}\Omega$ can be seen in the resistance ( $Z_{\text{real}}$ axis).....   | 17 |
| Figure 15 | Data showing the changes in cell internal resistance as the state of charge is increased towards cell runaway.....  | 18 |
| Figure 16 | A 10 Ah cell was heated in $25^{\circ}\text{C}$ increments until thermal runaway failure was observed above $150^{\circ}\text{C}$ . Impedance spectra data was collected between each temperature step. This shows a decrease in the internal resistance with each step up to $100^{\circ}\text{C}$ , followed by rapidly increasing internal resistance as the cell approached failure. .... | 19 |
| Figure 17 | Thermal abuse data applied for impedance monitoring seen in Figure 11. ....   | 19 |

|   |    |
|---|----|
| Figure 18 EIS data collected on 3s1p string with overcharge abuse on a single cell. The Nyquist plot (left) shows changes in the charge transfer resistance as the overcharge is increased, shown quantitatively to the right.....  | 20 |
| Figure 19 The quantitative charge transfer resistances from Figure 19, determined using a Randle equivalent circuit approximation. ....   | 20 |
| Figure 20 EIS data collected on 3S1P string with thermal abuse on a single cell. The abused cell was heated in 25 °C intervals and went into runaway at 175 °C. The Nyquist plot shows a rightward shift in the data at temperatures above 100 °C .....   | 21 |
| Figure 21 Quantified internal resistance values from Figure 21, showing a measureable increase above 100 °C .....   | 21 |
| Figure 22 Impedance data collected on a fully parallel string (1S3P) at various temperature steps of the thermal abuse of a single cell within the string. Nyquist plots are shown for the entire data set (left).....  | 22 |
| Figure 23 An expanded view showing changes in data as the temperature is increased .....  | 23 |
| Figure 24 A 10 Ah cell was heated continuously at 5 C/minute until cell failure with continuous impedance monitoring using the INL impedance measurement hardware.....  | 23 |
| Figure 25 Thermal ramp test performed during the impedance monitoring in Figure 24.....   | 24 |
| Figure 26 Impedance spectra of 3-cell parallel module collected during thermal ramp of a single cell. This data was collected using the traditional hardware, and shows a very constant impedance up to 100 C, followed by noticeable changes at 150 °C and above.....  | 24 |
| Figure 27 Impedance spectra of 3-cell parallel module collected during thermal ramp of a single cell. This was collected using the INL rapid-impedance test hardware and shows similar results to the traditional hardware (Figure 1). The impedance remains very constant up to 125 °C, followed by shifts at 150 °C and higher as the cell approaches runaway. .... | 25 |
| Figure 28 Continuous impedance testing performed during 5 °C/min thermal ramp with 60 second intervals between scans. ....  | 26 |
| Figure 29 Continuous impedance testing performed during 5 C/min thermal ramp with 20 second intervals between scans. ....   | 26 |
| Figure 30 Continuous impedance testing performed during 3 C/min thermal ramp with 20 second intervals between scans. ....   | 27 |
| Figure 31 Continuous impedance testing performed during 2 C/min thermal ramp with 20 second intervals between scans. ....   | 27 |
| Figure 32 Expanded view of Figure 31 above showing changes as the cell approaches runaway .....   | 28 |

## ACRONYMS

|     |  |
|-----|--|
| BMS | battery management system              |
| DOE | Department of Energy                   |
| EIS | electrochemical impedance spectroscopy |
| SNL | Sandia National Laboratories           |
| SOC | state of charge                        |
| SOH | state of health                        |
| SOF | state of functionality                 |
| IMB | impedance measurement box              |
| INL | Idaho National Laboratory              |
| SOS | state of stability                     |

# 1. INTRODUCTION

Traditional monitoring of electrochemical cells and batteries has been limited to observation of voltage and sometimes temperature of the cell or cells. While this monitoring can be very robust, there are limits to how predictive voltage and temperature behavior can be prior to a thermal runaway event. Ultimately, voltage and temperature changes are often lagging indicators or symptoms of battery failure, and by the time a noticeable change is detected it is too late to arrest cell failure with intervention or maintenance. Further, instantaneous voltage and temperature monitoring are often inadequate to determine the state of a battery at rest, particularly if the battery has been previously subjected to an abusive condition. Proper handling of a battery after an abusive event generally requires assuming the battery is potentially unstable and may yet undergo a thermal runaway event, venting or expulsion of contents. This usually requires full discharge and/or destruction of the battery after an abusive event whether a thermal runaway was observed or not. Knowledge of the level of stability of a damaged battery would allow for both safer and more efficient handling of the abused battery.

This work examines the application of electrochemical impedance spectroscopy (EIS) as a tool for determining the state of stability (SOS) of an electrochemical cell or battery. The cells for this study were subjected to thermal and electrical abuse coupled with EIS monitoring at differing levels of battery abuse. This aims to not only provide a deeper understanding of how abused cells and batteries fail, but also form the technical basis of a tool that could ultimately be used to interrogate cells of an unknown stability and even monitor active cells for early signs of damage or failure. These tests will look for markers within the EIS data that correspond to the onset of unstable conditions. These markers could then be potentially applied to interrogate batteries of an unknown stability as well as provide the basis for an active diagnostic method as part of a battery management system.

The primary drawback of traditional EIS is that it is typically not suited to measurements of dynamic systems due to the time involved to take a full measurement. This has historically limited the use of impedance measurements to either full spectra of stable systems, or dynamic measurements at a single high frequency, such as 1000 Hz. These have significant drawbacks, as limiting the measurement to stable systems would preclude any use as an on-board diagnostic tool, and single frequency measurements generally only yield limited information. Rapid-impedance techniques have been developed previously, but typically require expensive hardware and sophisticated data analysis to replicate the data obtained through traditional measurements. Idaho National Laboratories has developed a rapid-impedance tool that uses off the shelf parts. This tool is evaluated as part of this work, including both replicating the work performed with the traditional tool as well as collecting impedance data during dynamic conditions.

## 1.1. Stability of abused batteries

Abuse of electrochemical cells and batteries can have a wide range of effects depending on the type and severity of damage caused, as well as the properties of the battery itself. From a safety perspective, simple passive monitoring is often unable to identify the onset of failure until it is too late to intervene. Once a significant voltage change or self-heating of a cell is observed, a

catastrophic runaway of the cell is often inevitable [1-7]. The ultimate weakness of traditional monitoring techniques, typically based on voltage and temperature monitoring, is that they detect only the symptoms of a cell failure. Once a significant change has been registered, irreversible internal changes have likely already occurred within the cell. Compounding the issue is the fact that batteries have everything they need to release their stored energy inside the cell, meaning that once a catastrophic failure has initiated no amount of intervention can keep the reaction from proceeding to its conclusion. The prevention of catastrophic failure requires detection of internal faults well before they have developed to the point of no return. This makes techniques that can monitor the internal health of a cell essential to provide true protection from catastrophic failure. Further, many common forms of non-abusive field failure, such as internal short circuits, are the result of small defects that develop and exacerbate over time and are not readily detectible with conventional diagnostic tools at the time of a cell's initial construction. Monitoring changes to the impedance would aid in identifying ailing cells before a dangerous and costly failure.

Safety issues can be further compounded by the use of multi-cell modules. Monitoring of a pack of multiple cells with traditional techniques can be misleading as a pack that otherwise appears healthy may have a single problematic cell within the pack. Abusive conditions can also be unintentionally created, as voltage imbalance can create overcharge and overdischarge conditions while poor thermal design of a module can create thermally abusive conditions. A single cell undergoing catastrophic failure can cause cascading failures to other cells within the module.

These problems present a clear need to be able to detect and mitigate catastrophic cell failure under normal use and abuse conditions for transportation energy storage systems. Figures 1 through 3 show testing results for a series of lithium-ion cells under overcharge, mechanical penetration, and thermal abuse conditions, respectively. Under each abuse scenario, the failure events are preceded by a cascading sequence of decomposition reactions that are a challenge to monitor using passive temperature and voltage measurements. In general, voltage and/or temperature signatures indicative of failure are measured well after the point where these degradation reactions can be arrested and a failure event could be prevented.

Figure 1 shows an overcharge abuse test of a lithium-ion cell at 2C. In the region between 100 and 125% SOC the cell voltage increases by <400 mV and the temperature increases by 25 °C. At 125% SOC, there is an inflection in both the voltage and temperature response of the cell, indicative of eminent, unstoppable failure. The cell becomes highly resistive and the cell voltage reaches the charging compliance voltage which is followed by a high rate runaway and cell failure.

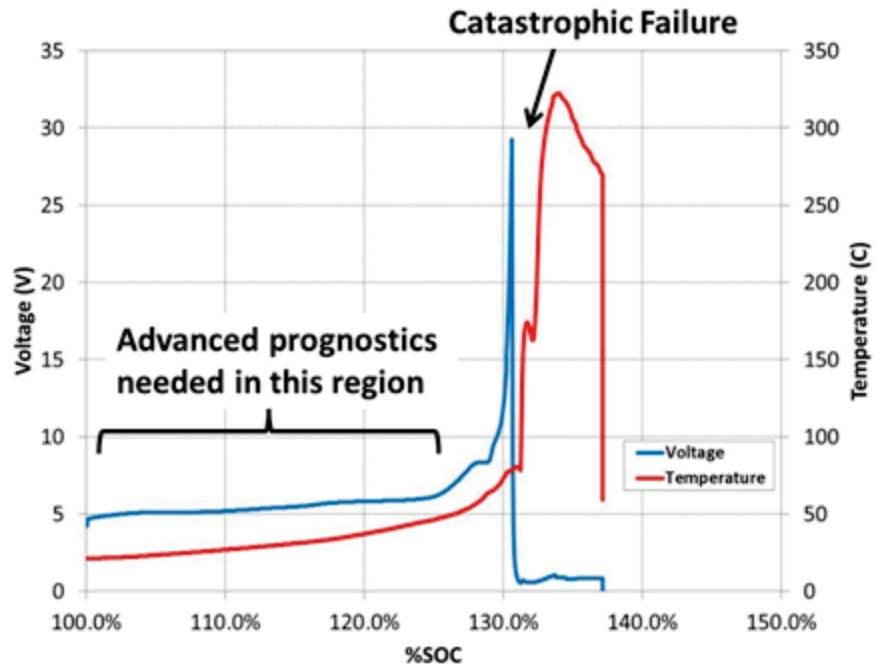


**Figure 1** Cell voltage and skin temperature as a function of state-of-charge during a 2C overcharge test of a 12 Ah lithium-ion cell.

In a slow speed, mechanical penetration experiment, there can be almost no passive warning signs prior to cell failure, shown in Figure 2. A cell is penetrated at 0.02 mm/s and shows no voltage drop or temperature rise during the first 4 mm of intrusion (up to 350 s). Once the cell package is ruptured, the cell short circuits and immediately goes into thermal runaway. Similarly, there is very little warning for a cell that develops an internal short circuit over time in the field because of a manufacturing defect or flaw which leads to a failure event [8]. During a thermal abuse scenario (Figure 3) there is a clear onset point of cell self-heating at 150 °C prior to a thermal runaway event. However, once appreciable self-heating is initiated it is practically too late to avoid a runaway reaction. In all of these abuse scenarios with conventional lithium-ion cell chemistries, rapid response, embedded sensors to measure internal cell degradation along with control strategies to remove the abuse and mitigate failure are essential. Early detection and prevention are critical for arresting these cascading degradation reactions that lead to an unstoppable runaway failure event.

Current state-of-the-art in battery monitoring for both industrial and on road motive power applications falls far short of the capability to detect impending battery failure. Rather, the state-of-the-art simply provides for operating the battery within a set of prescribed conditions to maintain optimal performance. Battery failures are detected only if they occur over a prolonged period and impact overall battery performance. Rapid failures are neither detected nor mitigated in the current state-of-the-art.

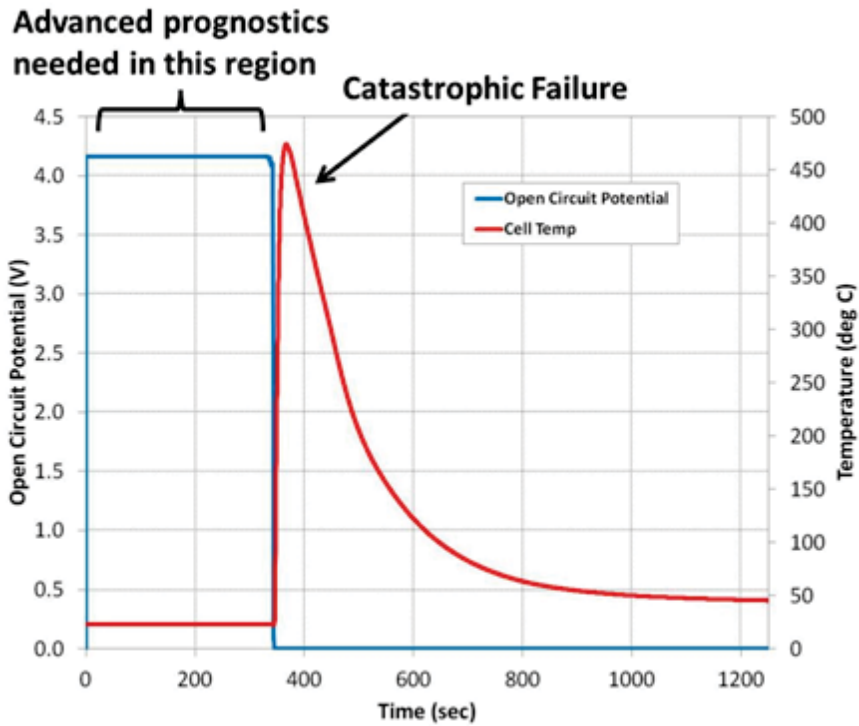


**Figure 2** Cell voltage and skin temperature as a function of time during a blunt-nail penetration test of a 2 Ah 18650 cell

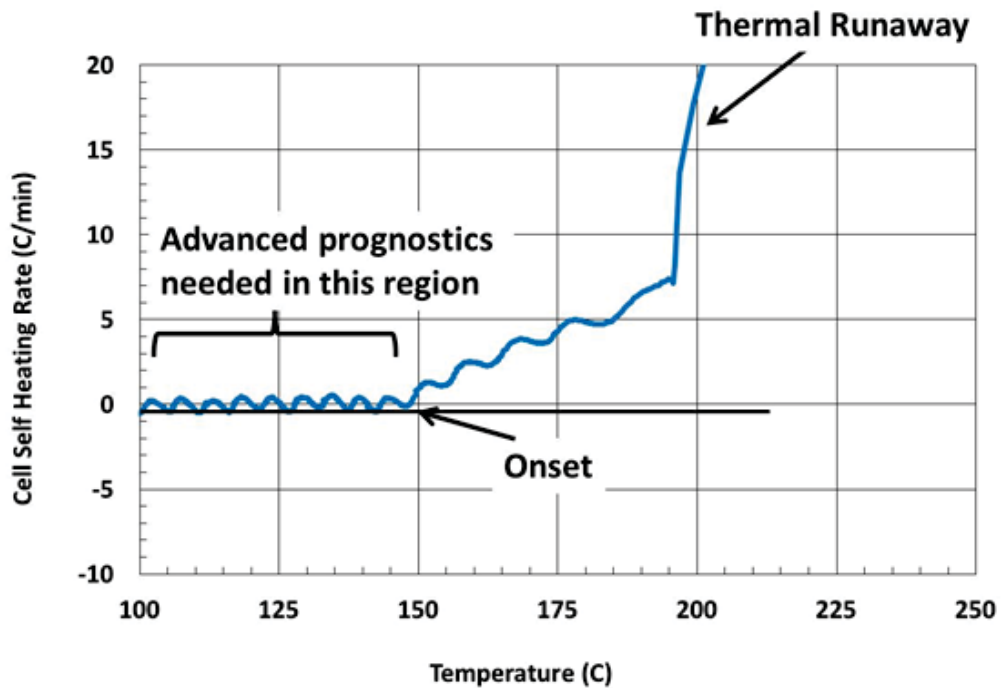


**Figure 3** Cell self-heating rate ( $^{\circ}\text{C}/\text{min}$ ) as a function of temperature of a 2 Ah 18650 cell during a thermal ramp test at ramp rate of  $5^{\circ}\text{C}/\text{min}$

## 1.2. Electrochemical impedance spectroscopy

EIS measurements have been emphasized as a valuable tool for battery modeling and life estimation [9-13]. EIS data have been shown to reveal changes in the bulk behavior of the electrochemical processes as well, which can give an indication of the changes in the battery electrode surface and diffusion layer [14]. With half-cells (i.e., using a reference electrode to isolate the individual effects of the anode and cathode during measurements [15], offline impedance measurements could also be a valuable diagnostic tool in assessing the degradation of the individual electrodes [16]. However, it has not been typically considered useful for online monitoring systems since the equipment is usually very expensive and the measurement duration is relatively lengthy. Standard EIS measurements usually consist of sequentially sweeping through a given frequency range by injecting sinusoidal excitation signals into the battery (or other energy storage device) and capturing the response. Depending on system settings and the frequency range, the impedance measurement sweep could last somewhere between 10 minutes to one hour or more, which is not well suited for onboard applications.

EIS is increasingly being used as well for estimation of the state of health (a measurement of performance degradation) and state of charge of batteries. Fleischer et al. [17, 18] have described algorithms for modeling the level of functionality based on parameters measured by the BMS. They suggest the use of EIS to monitor the charge transfer resistance, but concede it was likely not feasible due to the hardware necessary to collect impedance data. Impedance measurements have also been used to monitor changes to internal temperature of cells. Srinivasan et al. [19] as well as Schmidt et al. [20] have correlated impedance measurements to the internal temperature of an electrochemical cell and used empirical correlations to allow single frequency impedance measurements to serve as a means to monitor individual cell temperature.

Recent work has also used EIS to examine the changes in cells in light to moderate levels of abuse. Love et al. have examined the impact of overcharge on the single frequency impedance of single cells [21] as well as 4 cell series strings [22]. This was able to find a measurable shift in the 500 Hz impedance data as a cell was overcharged up to 135% total SOC. Single frequency impedance has the advantage of being easily integrated into a system as it does not necessarily require costly hardware or computing analysis. Also, at higher frequencies it can be measured very quickly to provide a real-time measurement.

Single frequency measurements are capable at measuring shifts in the internal resistance, such as those caused by solid electrolyte interphase (SEI) breakdown or damage to the separator, but those specific frequencies would need to be carefully selected as the whole spectra can shift with aging. Changes in other quantities, such as the charge transfer resistance and the conductivity of the battery electrolyte may show shifts in the complex impedance spectrum but little change in a single frequency analysis. This is particularly true if the single frequency analysis is at a relatively high frequency, as many phenomena only become apparent at lower frequencies.

A typical Nyquist curve measured from a commercially available lithium-ion cell is shown in Figure 4. The high frequency tail on the left side of the spectrum at frequencies greater than 251.2 Hz typically captures equipment artifacts [22] and is not shown in this figure. The point at which the high-frequency tail crosses the real axis is the ohmic resistance ( $R_o$ ) within the battery,

which includes the effects from the electrolyte, electrodes, tabs, etc. The semicircle in the mid-frequency region identifies the effective charge transfer resistance ( $R_{CT}$ ), which is primarily influenced by the kinetic reactions at the electrodes due to an imposed constant voltage or current signal. The low-frequency tail on the right is known as the Warburg impedance that is caused by the diffusion of ions [15, 23]. The semicircle trough, identified at 1.26 Hz, is the measured transition point between the mid-frequency charge transfer resistance and the low-frequency Warburg tail. These data show changes in the bulk behavior of the electrochemical processes and can provide valuable insight into battery degradation mechanisms during aging.

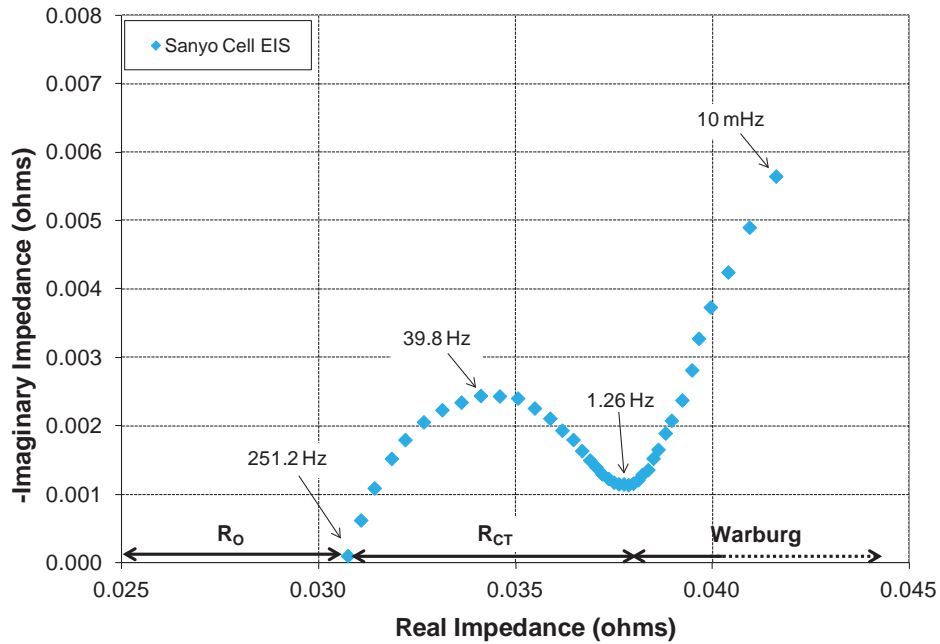


Figure 4 Impedance spectrum Nyquist curve [22]

### 1.3. Rapid-impedance measurement tools

INL, in collaboration with Montana Tech of the University of Montana, has developed a prototype sensor to improve the overall accuracy and reliability of SOH assessment techniques for electrochemical energy storage devices. The principle of operation for this impedance measurement box (IMB) is to capture impedance spectra rapidly over a broad frequency range using simple hardware and control software that processes unique algorithms to determine the spectra based on a sum-of-sines excitation signal. Various rapid-impedance spectrum measurement techniques have been developed to yield high resolution data comparable with standard, COTS equipment (i.e., multiple data points within the impedance spectra). Harmonic compensated synchronous detection (HCSD) is an example of rapid, lower resolution impedance measurement technique [22, 24, 25]. The sum-of-sines excitation signal consists of frequencies that are separated by octave harmonics so as to eliminate the effects of crosstalk interference. With no crosstalk error, the duration of the excitation signal needs to be only one period of the lowest frequency. Thus, given a frequency range of 0.1 to 1638.4 Hz with 15 frequencies included within the sum-of-sines excitation signal (i.e., 0.1 Hz, 0.2 Hz, 0.4 Hz, 0.8 Hz, etc.), the measurement duration would only be ten seconds long. The overall battery response to the excitation signal is captured and then synchronously detected at each frequency

of interest to determine the impedance spectrum. The analysis methodology is relatively computationally simple using synchronous detection without the need to compensate for crosstalk error and could be implemented as an embedded software analysis tool.

First-generation prototype IMB systems, shown in Figure 5, were built for preliminary validation and demonstration testing, the results of which are provided below. This first-generation system was built for cell-level measurements ( $\leq 5$  V) and the data acquisition system required an interface with a standard desktop computer to operate the control software. A second-generation system was subsequently built for cell-level studies, but reconfigured to be a portable system with a lower cost data acquisition card that could interface with a laptop. A prototype third-generation system has also been recently designed as shown in Figure 6 (the system is connected to a commercially available 12 V lead-acid battery in this image). Several enhancements have been made to the Generation 3 hardware system, including an applied dynamic range between 0 and 50 V for a cell- or module-level battery measurement, voltage and current probe protection, reduced noise crosstalk in the voltage feedback loop, modular design, and a significantly improved calibration technique. All three IMB generations were designed with filters capable of measuring frequencies up to 2 kHz, which is generally sufficient for battery impedance measurements.



**Figure 5** Generation 1 IMB

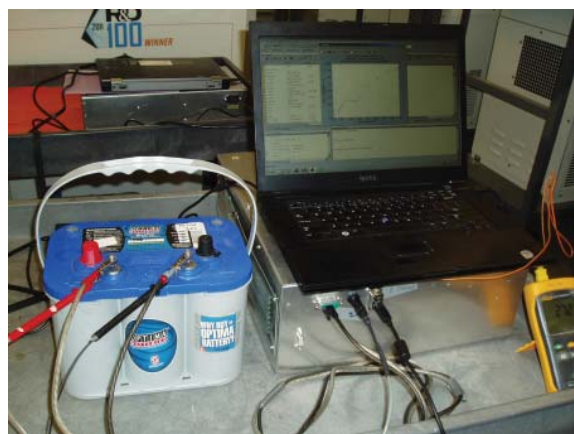


**Figure 6** Generation 3 IMB attached to a 12 V lead-acid module

Because battery failure under abusive conditions occurs rapidly (several seconds to 10s of seconds) and can be destructive to the cell, analysis is typically limited to what can be passively measured in real-time or what can be gleaned from the aftermath of a test. Measurement of impedance changes in failed cells is typically a before-and-after scenario or not realistically possible due to the physical state of the cell after testing. The IMB sensor development may, however, also be used for rapid online assessment of battery failure mechanisms, allowing for in-situ characterization of impedance changes of a cell during failure and potentially lead to a greater understanding of the mechanisms of battery failure so as to prevent catastrophic events.

The successful development of a rapid-impedance spectrum sensor that can help to improve the overall safety and reliability of batteries in addition to creating an opportunity for improved power management, monitoring, and control could significantly leapfrog existing approaches and have a positive impact on both technology and business aspects. For example, improved safety mitigation and control can help to reduce the potential for fires caused by thermal runaway that can result from conditions ranging from cell defects to automotive crashes.

## 2. EXPERIMENTAL METHODS

A LiCoO<sub>2</sub>-based cell chemistry was chosen as it is well studied and the thermal runaway behavior of these chemistries is well known. Tests were performed on 10 Ah AA Portable Power Corp. cells, model # 9759156-10C, obtained from [www.batteryspace.com](http://www.batteryspace.com). The cells are pouch format cells with a nominal operating voltage of 3.8 V and a charge-discharge range of 2.75 V to 4.2 V. The rationale behind this cell choice was that they are of a capacity that is reasonably close to the single cells found within EV battery systems, albeit at the lower end of the common range. Impedance testing, except where the INL rapid-impedance tool was used, was performed using a Solartron Modulab potentiostat, frequency response analyzer and 2 A current booster.

### 2.1 Single-cell testing

Single-cell testing was performed to examine the impedance response to thermal ramp and overcharge. To facilitate impedance testing, tests were performed in a stepwise manner, allowing the cell to equilibrate at different levels. Impedance data was collected from 1 kHz to 0.1 Hz in galvanostatic mode, with a perturbation current of 2 A.

#### 2.1.1 Single-cell overcharge testing

Overcharge testing was performed on cells starting at 100% SOC. The cells were charged at 10 A (1C nominal rate) to 20% overcharge increments. At each 20% increment the cell voltage was allowed to stabilize and an impedance measurement taken. After completion of the impedance measurement the overcharge was resumed until the next 20% of overcharge was reached. This was continued until cell failure was observed.

#### 2.1.2 Single-cell thermal ramp testing

Thermal ramp testing was performed on cells at 100% SOC. Beginning at room temperature, cells were heated in increments of 25 °C. After each increment of 25 °C the cell temperature was allowed to stabilize and an impedance measurement taken. After completion of the impedance measurement the overcharge was resumed until the next 25 °C increment. This was continued until cell failure was reached.

### 2.2 Three-cell string testing

Strings composed of three of the above cells were tested as well. The cells were connected in fully series (3S1P) and fully parallel (1S3P) configurations. For these test the abuse condition was applied on a single cell within the string while the impedance measurement was made on the entire string. In all cases electrical connections were made by welding 0.127mm × 5.08mm (0.005" × 0.200") nickel ribbon to the battery tabs. The abused cells were constrained in all tests. Overcharge testing was constrained using 12.7mm (½") phenolic board, while during thermal ramp tests constraint was provided by the brass heater blocks also used to apply heat. The other two cells in the string not subjected to abuse conditions were not constrained. These cells were also given enough physical separation so that heating of the abused cell did not impact the other cells in the string.

### *2.2.1 Series testing (3S1P)*

Series strings were constructed by connecting three of the 10 Ah cells tested above together in series. The pack together had a nominal operating voltage of 11.4 V and nominal capacity of 10 Ah. The operating voltage window was 8.25 V to 12.6 V. Testing on the series modules included single-cell overcharge tests as well as single-cell thermal ramp tests. The impedance testing was performed with the Solartron potentiostat as above, but with the addition of a high voltage booster module to allow for testing at the elevated pack voltage. Impedance testing was collected in galvanostatic mode with a signal current of 2 A. The spectrum was collected from 1 kHz to 0.1 Hz.

Overcharge testing was performed by applying an overcharge current to a single cell within the series string. Similar to the single cell tests, the overcharge cell was charged starting with all cells in the string at 100% SOC. The overcharged cell was then charged in 20% SOC increments. After each 20% increment, the string voltage was allowed to stabilize and an impedance spectrum was collected on the entire string. This was continued until cell failure was observed.

Thermal ramp testing was performed by bringing a single cell within the string into thermal runaway with periodic impedance data collection. Starting at 25 °C a single cell within the string was heated in 25 °C increments. After each heating step the cell temperature was allowed to stabilize and an impedance measurement made on the entire string. This was continued until cell failure was observed.

### *2.2.2 Parallel-string testing (1S3P)*

Fully parallel strings of three cells were constructed using the 10 Ah pouch cells above. The string as constructed had a nominal operating voltage of 3.8 V with a charge capacity of 30 Ah. The operating voltage window was 2.75 V to 4.2 V. Testing on the parallel strings focused on thermal abuse testing as a parallel electrical configuration does not allow for the overcharge of a single cell.

Thermal abuse testing was performed by affixing brass heater blocks to a single cell of the string. The cells were then heated starting at 25 °C in 25 °C increments up to 150 °C. After each heating step the temperature was allowed to stabilize and an impedance measurement taken. After reaching 150 °C the abused cell is heated in 10 °C increments, with stabilization and impedance measurements taken between each step. These steps were continued until failure of the abused cell was observed.

## **2.3 Testing with the INL rapid-impedance measurement tool**

A rapid-impedance measurement tool developed at Idaho National Laboratory was tested by performing tests similar to those above. The INL tool is designed for rapid collection of impedance data and is described in more depth above (Section 1.3). Testing focused on single cell overcharge and thermal abuse testing, as well as parallel-string thermal abuse testing. The available unit for this research effort had a maximum operating voltage of 5 V, so series string tests were not performed.

The INL tool was tested in two primary modes of operation. The first examined it as a stand-alone replacement for the traditional impedance measurement tool. Single-cell overcharge and

thermal abuse tests, as well as parallel-string thermal abuse tests were conducted as above (Sections 2.1, 2.2.2) using the INL tool. Due differences in operation, slightly different impedance parameters were used. The device was operated with a maximum signal current of 2 A with a frequency window of 0.05 Hz to 1580 Hz. The abuse tests were conducted in the same manner as above.

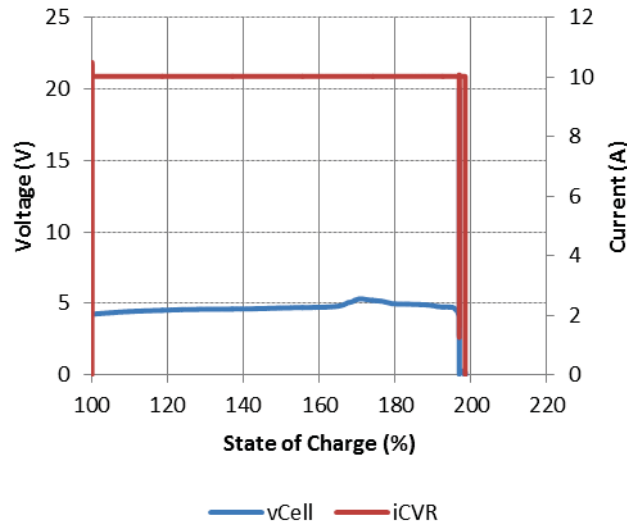
The INL tool was also tested in a continuous operation mode. This was performed entirely with thermal abuse testing, as currently the control software had not yet been optimized to operate with an active load, which would be necessary for continuous overcharge testing. Single-cell testing was performed by attaching brass heater blocks to the cell and applying a temperature ramp rate of 5 °C/min to the cell. Each impedance measurement took 20 seconds, followed by a 20-second settling time. The INL tool was allowed to collect these measurements until cell failure.

The 1S3P test was set up as described in Section 2.2.2. The response of the parallel string was tested at varying thermal ramp rates of 2 °C/min to 5 °C/min. During the thermal ramp test the INL tool was used to collect impedance measurements throughout the tests. The effects of different settling times between each measurement were examined as well.

### 3. RESULTS

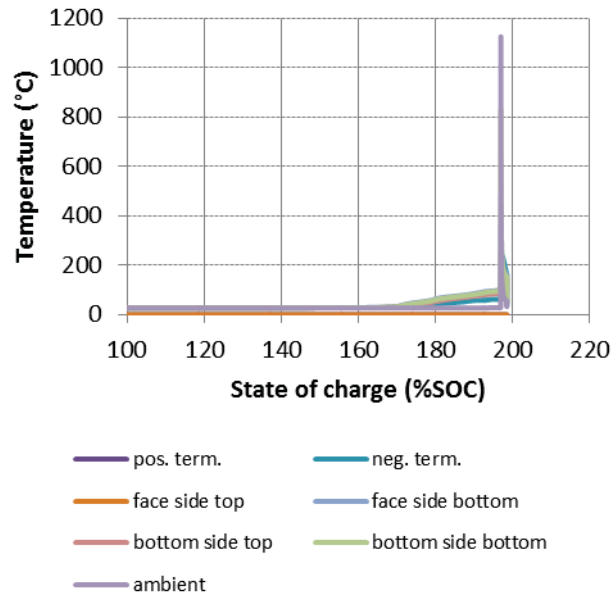
#### 3.1 Cell selection, validation and initial testing

The cells were subjected to standard overcharge and thermal ramp tests per the USABC Abuse Testing Manual [26] to understand the baseline abuse response of these cells, with the data shown in Figures 8-10 below.



**Figure 7** Voltage and current during 1C rate (10 A) overcharge of 10 Ah prismatic pouch cell. Cell failure can be seen at ~198% SOC.

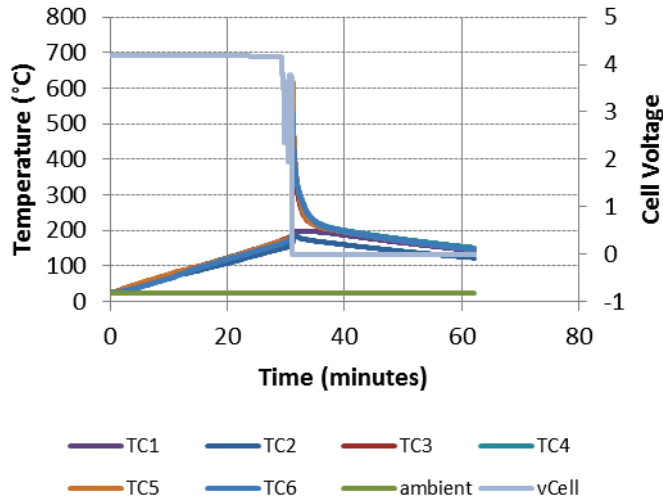
Figures 7 and 8 show overcharge abuse results collected on the 10 Ah pouch cells. The test shown is a 10 A (1C nominal rate) overcharge using a 20 V maximum compliance voltage. The cell shown has an energetic thermal runaway occurring at 198% SOC, with voltage and current both dropping to 0 as the power supply can no longer control current into the cell and temperatures as high as 1,113 °C observed on the surface of the cell. The voltage data shows a steady rise up to 165% SOC followed by a steeper increase then a loss of cell voltage as the cell progresses towards thermal runaway. The observed cell temperatures stay fairly close to ambient levels up to ~165-170% total SOC. At this point the temperatures begin to rise steadily until the onset of thermal runaway, where the cell rapidly spikes from a maximum observed temperature of 105 °C to a peak observed temperature of 1,110 °C, at which point the temperature rapidly declines as all stored energy of the cell has been expended.



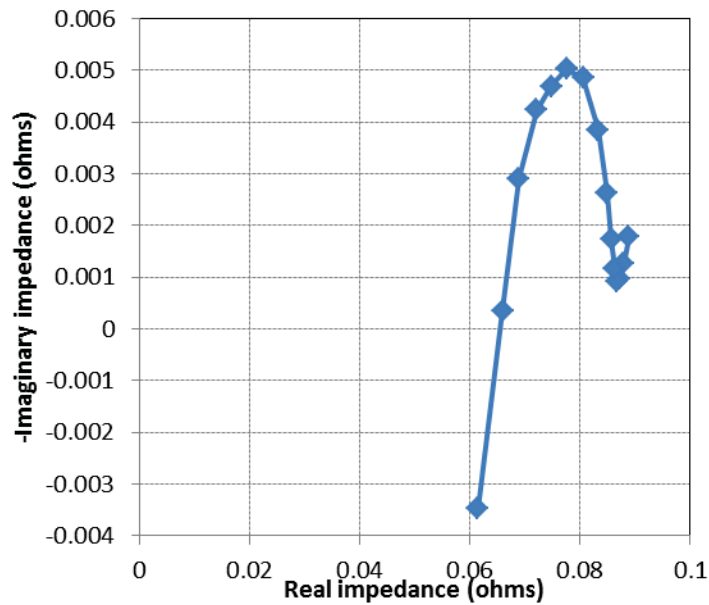
**Figure 8** Cell temperatures during 1C rate (10A) overcharge of 10 Ah prismatic pouch cell. Maximum temperatures during cell failure were observed as high as 1,113 °C.

Figure 9 shows the results of a thermal ramp abuse test. Thermal runaway is observed in the cell starting at 171 °C with a maximum observed cell temperature of 617 °C. The cell voltage is observed to hold fairly constant until a cell temperature of ~140 °C at which point a gradual decline in the observed cell voltage begins. This changes to a sudden and sharp loss of voltage corresponding to the onset of thermal runaway, at which point the voltage rapidly drops to effectively 0 V. As with the overcharge test above these results are emblematic of a cell that undergoes a rapid thermal runaway during which the bulk of the stored energy in the cell is released. The cells do however show signs of heating before the thermal runaway occurs as the cell begins to break down. These temperature changes may be difficult to spot outside of a laboratory environment. These pre-runaway regions are those that are ultimately of the most interest for advanced diagnostic techniques, where damage and decomposition may be occurring within a cell but the any failures are not yet so severe that the ultimate problem cannot be addressed.

The INL impedance measurement tool was also installed and validated. This included the travel of INL personnel to Sandia for installation, validation and training on the use of the equipment. The equipment was validated by collecting measurements on commercial-off-the-shelf 18650 cells to determine the operability and repeatability of the device prior to any testing at Sandia. Figures 10-11 show a sample of the results from validation testing of the impedance measurement hardware on a Panasonic CGR 18650 lithium ion cell, used for validation of the impedance equipment only. Figure 11 shows initial collection of impedance data using a 10 second collection time on a commercial 18650 lithium ion cell.



**Figure 9** Cell temperatures and voltage during thermal ramp test of 10 Ah prismatic pouch cell. Onset of thermal runaway occurred at ~171 °C with observed temperatures up to 617 °C.



**Figure 10** Validation testing of INL impedance measurement hardware showing EIS data for a commercial 18650 cell.

The repeatability of the measurements were tested by collecting 10 separate measurements on the same cell with the above parameters and compared to each other for any drift between tests. These are plotted in Figure 11 below showing little change between each measurement.

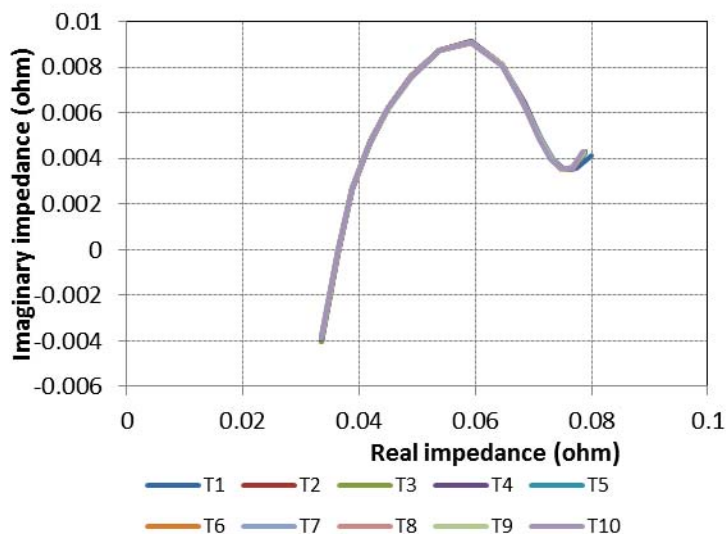


**Figure 11** Validation testing of INL impedance measurement hardware showing little drift in EIS data collected over 10 separate measurements of a cell under the same experimental conditions.

### 3.2 Single-cell overcharge testing

Work proceeded on the diagnostic testing of single 10 Ah cells. Figures 12-14 show the results obtained by collecting electrochemical impedance data at 20% charge intervals during overcharge testing. Overcharging was begun on a cell at 100% SOC at a 10 A(1C nom) rate. The overcharging was paused at 20% SOC intervals (12 minutes of 10 A charge) to allow for impedance data collection. Figure 13 shows the impedance data collected at the increasing charge intervals. The most notable feature of this data is the semicircle observed, the size of which is typically interpreted as the charge transfer resistance and initially decreases in magnitude from 100 to 120% SOC and further from 120 to 140%. This behavior is typical for a battery under an increasing state of charge. The behavior begins to change above 140% overcharge, however, as the data at 160% shows a larger magnitude, while at 180 and 200% overcharge this disappears completely. The nearly straight lines observed at these higher states of overcharge are consistent with the behavior of a resistor.

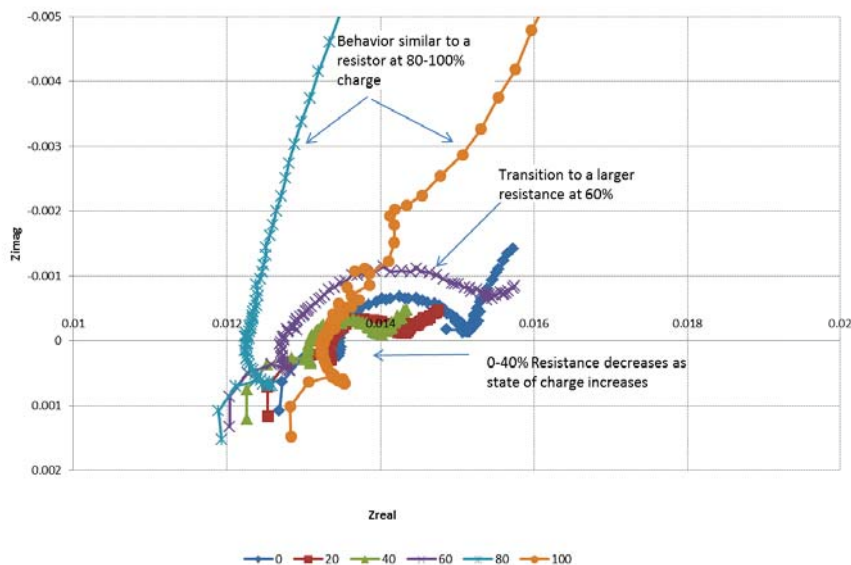


**Figure 12** Impedance data collected from 100% to 200% SOC prior to cell failure.

This can be correlated somewhat to the temperature data as seen in Figure 13. The temperature remains near ambient up to  $\sim 160\%$  SOC. After this point the cell temperature begins to ramp up quickly as it approaches failure. This provides a clear transition in the data pointing towards a cell that has reached a dangerous level of overcharge. This shows promise that impedance diagnostic techniques may be used to determine when a battery has undergone an irreversible change to its chemistry, resulting in an unsafe condition.

Figure 14 examines the potential repeatability of the measurement on multiple cells. The two cells examined show very similar behavior; however there is an offset in the resistance (x-axis) of the measurement of  $\sim 8$  mOhm. This is likely due to a small difference in the wiring resistance between the two tests. The potential for this shift in the data would need to be accounted for in any system that takes advantage of the observed changes in the impedance behavior.

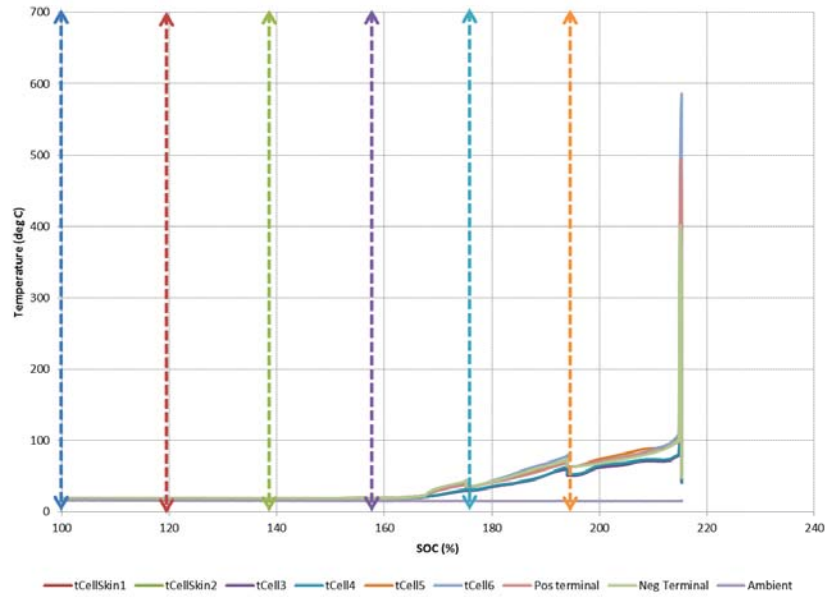


**Figure 13** Temperature data as a function of total state of charge. The cooling observed at ~180% and ~200% was due to cooling that occurred during the halt of overcharge testing. The dashed arrows show the corresponding points of data collection.

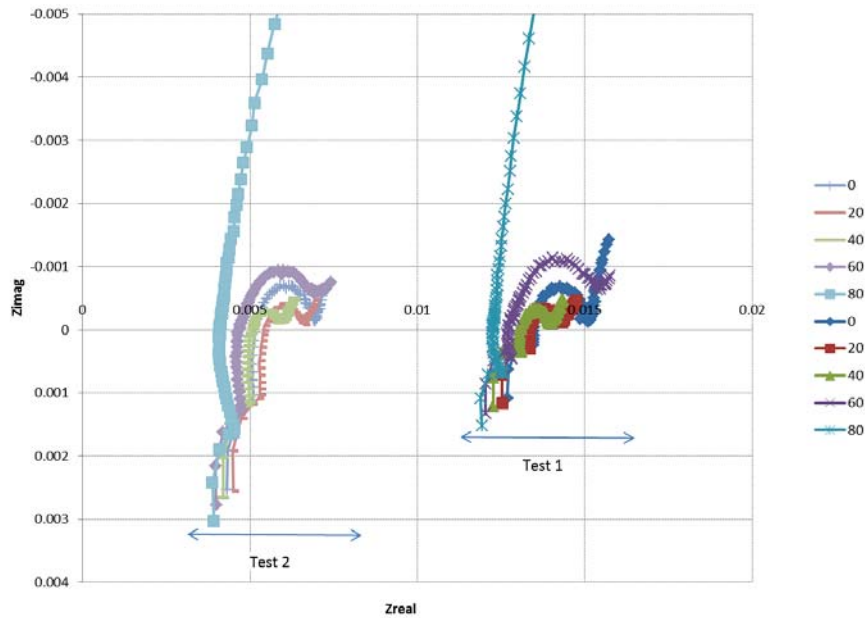


**Figure 14** Impedance data of two overcharge tests showing potential repeatability of measurements. While the general behavior of the two tests is very similar a shift of ~8 mOhm can be seen in the resistance (Zreal axis).

In Figure 15 the internal battery (ohmic) resistance has been extracted from the impedance data and compared to the cell temperature as it approaches runaway. The internal ohmic resistance

remains relatively constant at lower states of overcharge, however it begins to decrease at high levels of overcharge. The cell temperature remains near ambient temperatures at lower states of overcharge. Above 160% SOC the cell temperature begins to increase more rapidly until it enters thermal runaway.

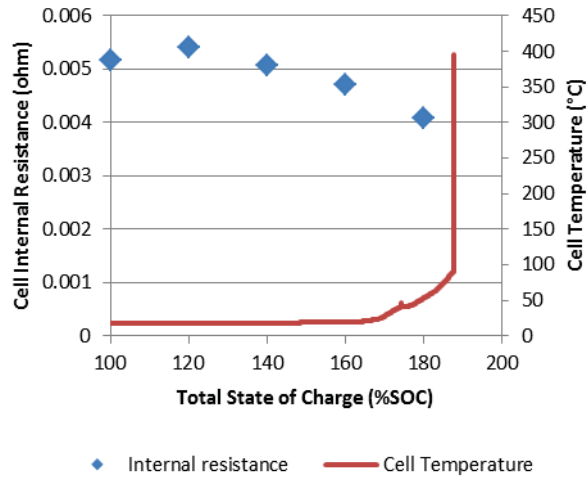


**Figure 15** Data showing the changes in cell internal resistance as the state of charge is increased towards cell runaway.

### 3.3 Single-cell thermal ramp testing

Thermal ramp analysis was performed on single cells using both traditional hardware as well as the INL rapid measurement hardware. The measurements with traditional hardware were performed by heating the cell in 25 °C increments. After each heating period the cell temperature was allowed to stabilize and impedance data collected. Selected test results can be seen in Figures 16 and 17 below. The impedance data (Figure 16) shows that the internal ohmic resistance (the x-intercept of the curve) decreases with increasing temperature up to 100 °C. As the temperature increases to 125 °C the internal resistance increases significantly, and increasing further as the temperature reaches 150 °C. In the next step thermal runaway occurs during temperature stabilization at 175 °C.

The cell voltage and temperature data are plotted as well in Figure 18. Most notably, it can be observed that the changes in the voltage as the cell approached the runaway temperature were fairly small until runaway was actually observed. This would be disguised further if the cell were included as a single cell within a larger battery pack. The changes in the impedance data as the temperature approaches unsafe levels are much more dramatic, and potentially make it easier to identify a developing problem within a cell before a catastrophic failure occurs.

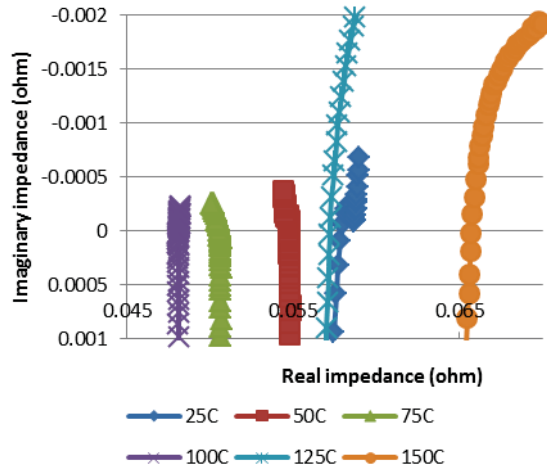


**Figure 16** A 10 Ah cell was heated in 25 °C increments until thermal runaway failure was observed above 150 °C. Impedance spectra data was collected between each temperature step. This shows a decrease in the internal resistance with each step up to 100 °C, followed by rapidly increasing internal resistance as the cell approached failure.

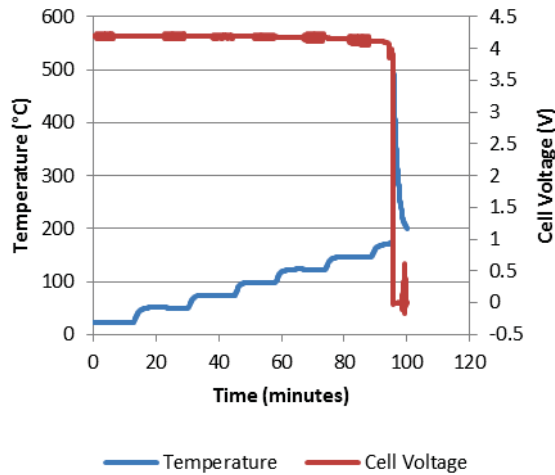


**Figure 17** Thermal abuse data applied for impedance monitoring seen in Figure 11.

### 3.4 Three-cell string overcharge testing

The overcharge tests were performed by applying 20% State of charge increments to a single cell with whole pack impedance measurements taken after each charging step. Figures 18 and 19 shows representative EIS data collected during overcharge abuse of a single cell within a 3S1P string. Impedance data was collected as high as 180% total SOC, with the cell failing at 200% SOC. The Nyquist data (Figure 18) shows that the internal resistance remains largely unchanged over the overcharge test. There is a noticeable change, however, in the radius of the semicircle, typically interpreted as the charge transfer resistance. There is also a significant change in the Warburg tail at 180% SOC appearing much earlier in the Nyquist plot than for other levels of overcharge. The charge transfer resistance in this case was evaluated using a Randle circuit approximation and is shown in Figure 19. After an initial drop, the charge transfer resistance

decreases more gradually from 120 to 160% SOC followed by larger drop at 180%. While interpretation of the data is more subtle in this configuration, it is important to note that there is still a measurable shift as a single cell within the string approaches runaway.

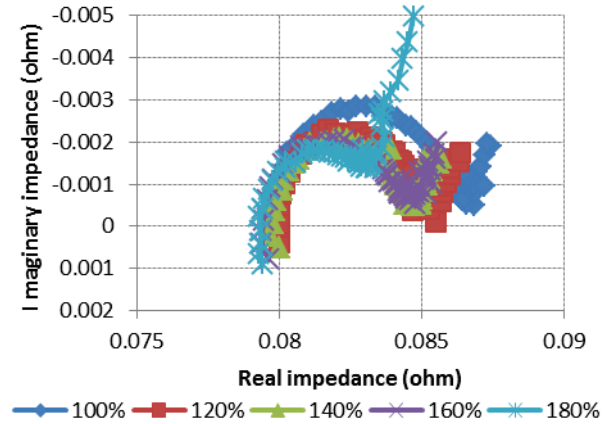


**Figure 18** EIS data collected on 3s1p string with overcharge abuse on a single cell. The Nyquist plot (left) shows changes in the charge transfer resistance as the overcharge is increased, shown quantitatively to the right.

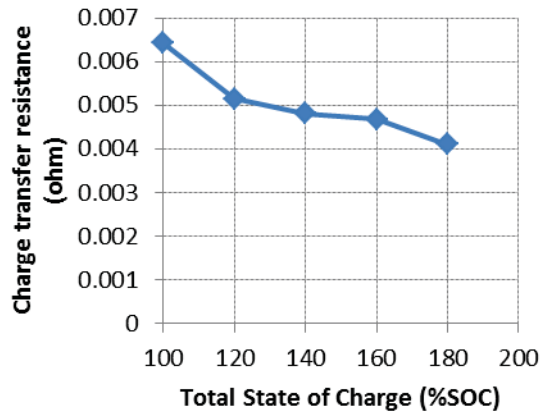


**Figure 19** The quantitative charge transfer resistances from Figure 19, determined using a Randle equivalent circuit approximation.

### 3.5 Three-cell string thermal ramp testing

Thermal ramp analyses were performed on three-cell series strings constructed with the single cells previously tested. The thermal ramp measurements were performed by heating a single cell of the string in 25 °C increments with impedance of the entire string taken after each heating step. All impedance measurements were performed over a frequency range of 0.1 to 1000 Hz.

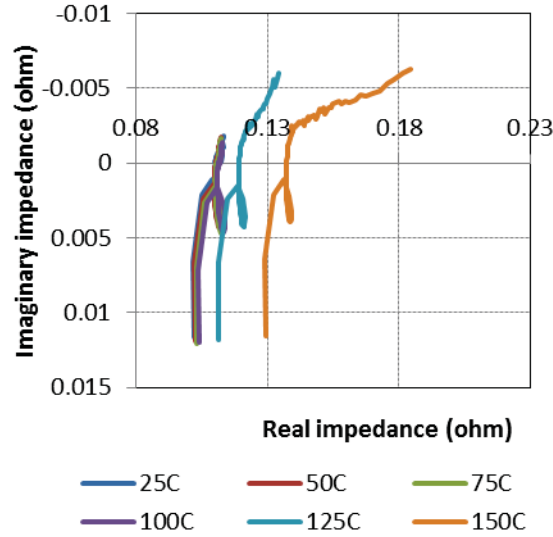


**Figure 20** EIS data collected on 3S1P string with thermal abuse on a single cell. The abused cell was heated in 25 °C intervals and went into runaway at 175 °C. The Nyquist plot shows a rightward shift in the data at temperatures above 100 °C

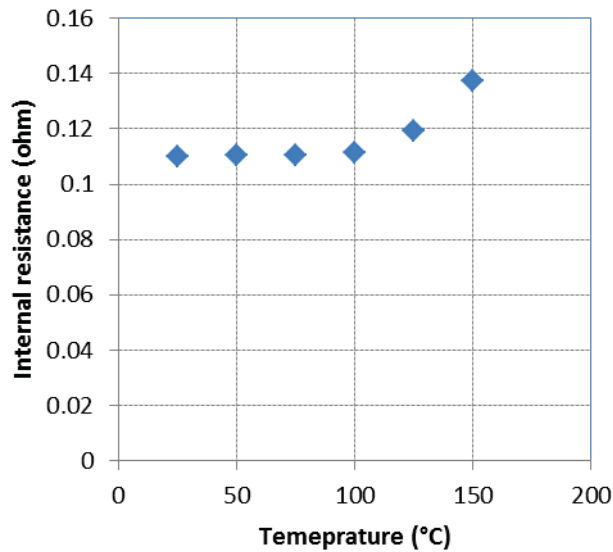


**Figure 21** Quantified internal resistance values from Figure 21, showing a measureable increase above 100 °C

Representative thermal ramp impedance data are shown in Figures 20 and 21. This shows similar behavior to that for single cells; the internal resistance remains very constant up to 100 °C, and begins to increase at higher temperatures. The internal resistance is plotted as a function of temperature in Figure 22. This shows a promising direct parameter change in series packs that can be used in a predictive way to monitor for potentially dangerous temperatures.

Three-cell parallel strings (1S3P) were constructed using the 10 Ah cells previously tested. The 1S3P strings were tested by applying thermal abuse to a single cell within the string with impedance measurements of the entire string taken at 25 °C intervals up to 150 °C at which point

impedance measurements were taken at 10 °C intervals until cell failure. The other cells in the string were kept thermally isolated from the abused cell to maintain them at ambient temperature throughout the test.

Representative impedance measurements taken after refinement of the tested string are shown in Figures 23 and 24. Scans of all temperature intervals can be seen in Figure 23 and there are two semicircle features observed in the data. The first, from  $R \sim 0.0025-0.00325$  ohm, shows little change as temperature increases. The second, meanwhile, remains very constant up to 100 °C, but then proceeds to show evidence of decreasing charge transfer resistance as the temperature increases above 100 °C. This is shown in more detail in Figure 24, where the expanded view shows very little change from 25-100 °C, but a noticeable shift as the temperature of a single cell is increased to 150-160 °C. The abused cell went into thermal runaway above 170 °C. These data illustrate that while the analysis is more challenging when working with parallel configurations, there is still a measurable change that occurs as the cell rises above safe operating parameters. Ideally this would provide the proper warning to arrest a thermal runaway before it progressed to a catastrophic failure.

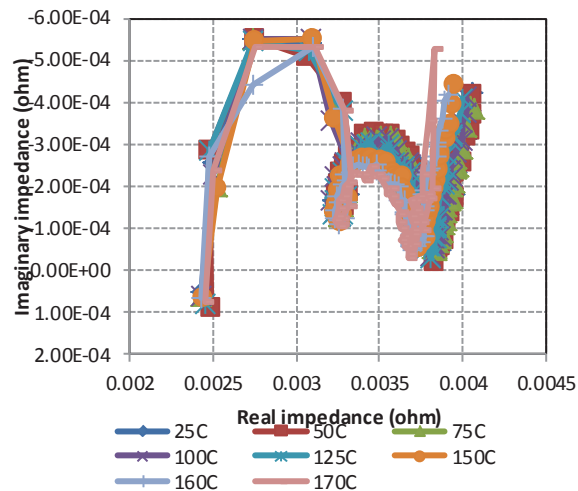


**Figure 22** Impedance data collected on a fully parallel string (1S3P) at various temperature steps of the thermal abuse of a single cell within the string. Nyquist plots are shown for the entire data set. The double loop observed appears to be related to the electrical connections between batteries and the first loop is very constant at varying temperatures.

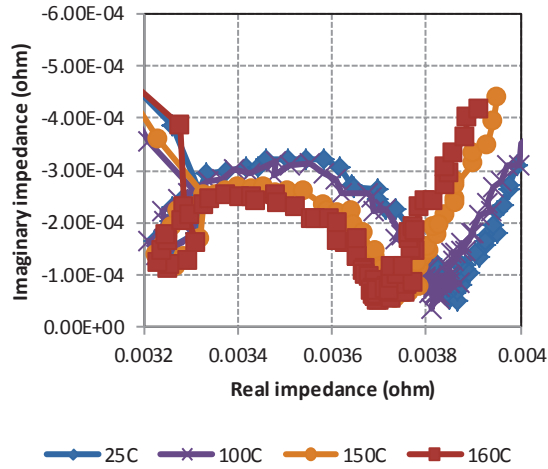


**Figure 23** An expanded view showing changes in data as the temperature is increased .

### 3.6 Evaluation of INL rapid-impedance measurement tool

Testing with the INL hardware was performed by applying a constant ramp rate of 5 °C/min to the cell being tested. During the constant heat rate impedance data was collected using the INL impedance measurement hardware. The data was collected using a frequency range of 0.1 Hz to 1580 Hz with a total collection time for each scan at approximately 12 seconds. Representative data with selected impedance data can be seen in Figure 24 below. Here behavior similar to that seen with the traditional hardware is observed. The internal resistance appears to remain relatively constant up to 100 C. After this point it begins to increase as the cell approaches runaway. While EIS data was collected during and after runaway as well, the cell was too damaged to provide valuable data.

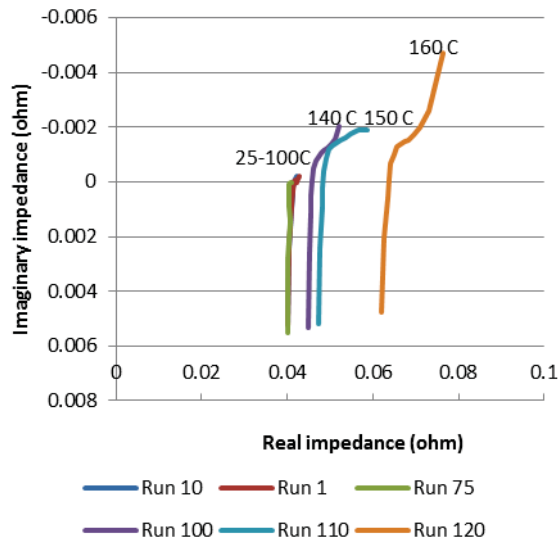


**Figure 24** A 10 Ah cell was heated continuously at 5 C/minute until cell failure with continuous impedance monitoring using the INL impedance measurement hardware.

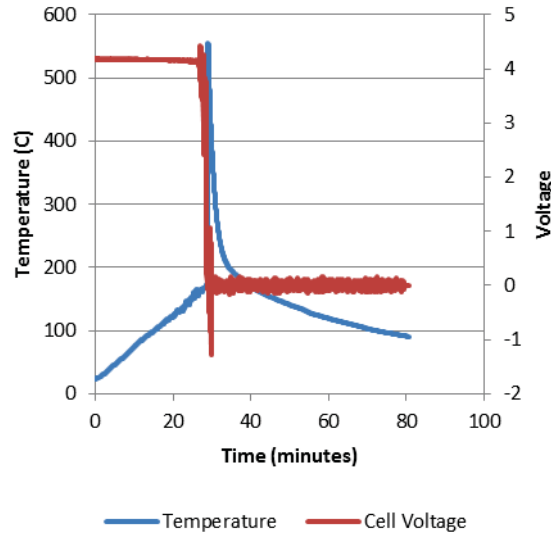


**Figure 25** Thermal ramp test performed during the impedance monitoring in Figure 24

Three-cell parallel packs were tested by applying a thermal ramp to a single cell within the pack, with impedance spectra collected for the entire parallel module. To compare the rapid-impedance tester with the traditional testing hardware, the temperature of the abused cell was increased in 25 °C increments from 25 to 150 °C, and then in 10 °C increments until thermal runaway occurred. The data using the traditional hardware is shown in Figure 26, with the data collected using the INL hardware is shown in Figure 27.

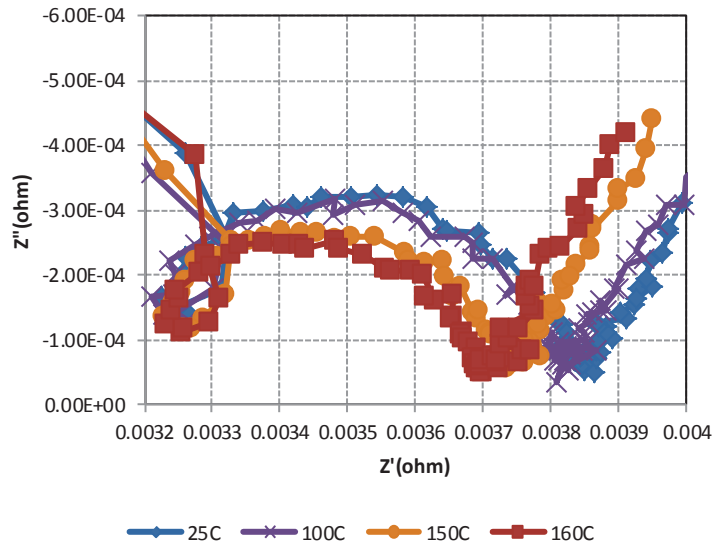


**Figure 26** Impedance spectra of 3-cell parallel module collected during thermal ramp of a single cell. This data was collected using the traditional hardware, and shows a very constant impedance up to 100 °C, followed by noticeable changes at 150 °C and above.

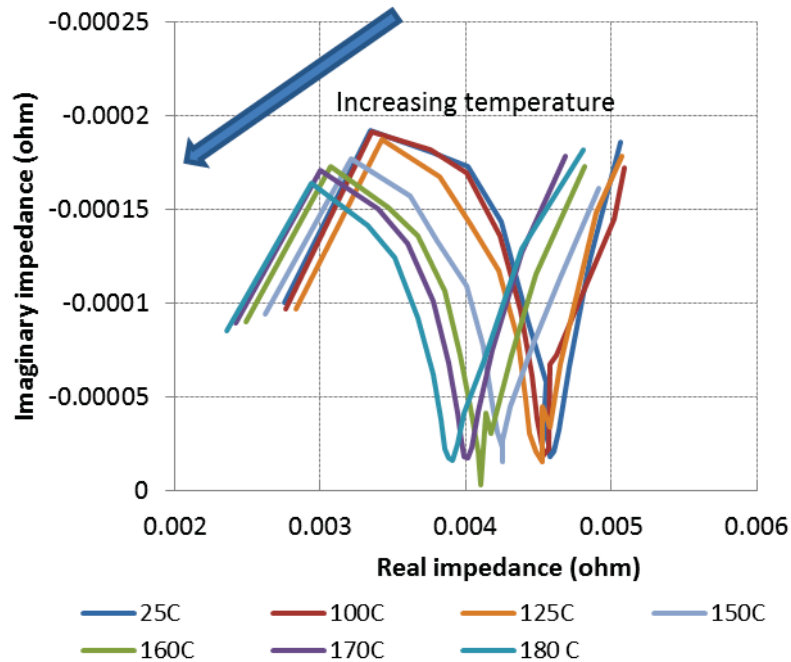


**Figure 27** Impedance spectra of 3-cell parallel module collected during thermal ramp of a single cell. This was collected using the INL rapid-impedance test hardware and shows similar results to the traditional hardware (Figure 1). The impedance remains very constant up to 125 °C, followed by shifts at 150 °C and higher as the cell approaches runaway.

While the rapid test hardware does collect fewer data points, the data sets collected using the different hardware show very similar results when using the same test method. The changes observed in the impedance are fairly small up to the 125 °C scan. Above that temperature, there is a change in charge transfer resistance (roughly the diameter of the observed semicircle). There is a significant shift as the temperature moves from 125 to 150 °C, followed by steady changes with each 10 °C increase as the cell approaches runaway. This shows not only a measurable change as the cell approaches runaway, but also good similarity between the two hardware types.

The next step of evaluating this method was to use the rapid-impedance hardware to evaluate a pack with one cell undergoing a continuous thermal ramp test. The abused cell was heated at a constant rate of 5 °C/min while the rapid test hardware made repeated impedance measurements of the pack. Representative data are plotted in Figures 28 and 29 below. The continuous scan data shows little change with increasing temperature, especially compared to the fairly noticeable changes observed when the temperature was stepped in increments and measurements taken after the temperature was allowed to equilibrate. Some possibilities for this difference are currently being considered. First, this study has not been previously performed, and it is possible that there were some equipment limitations that need to be addressed. Another possibility is that the heating rate is fast enough that the cell never sees equilibrium at any given temperature, so the transient state is driving the impedance result. This does illustrate the need that as this technique matures, the real-world conditions under which these tests will be conducted must be determined, and to ensure the technique will remain applicable under those conditions.

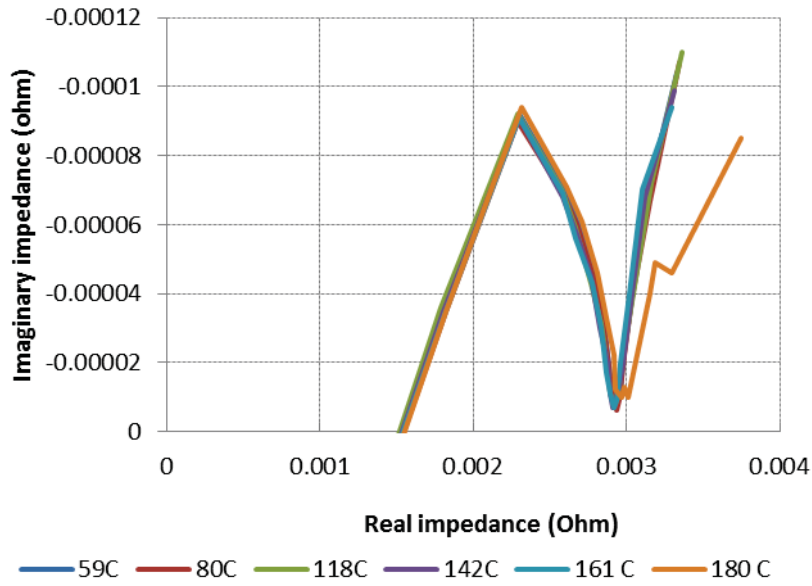


**Figure 28** Continuous impedance testing performed during 5 °C/min thermal ramp with 60-second intervals between scans.

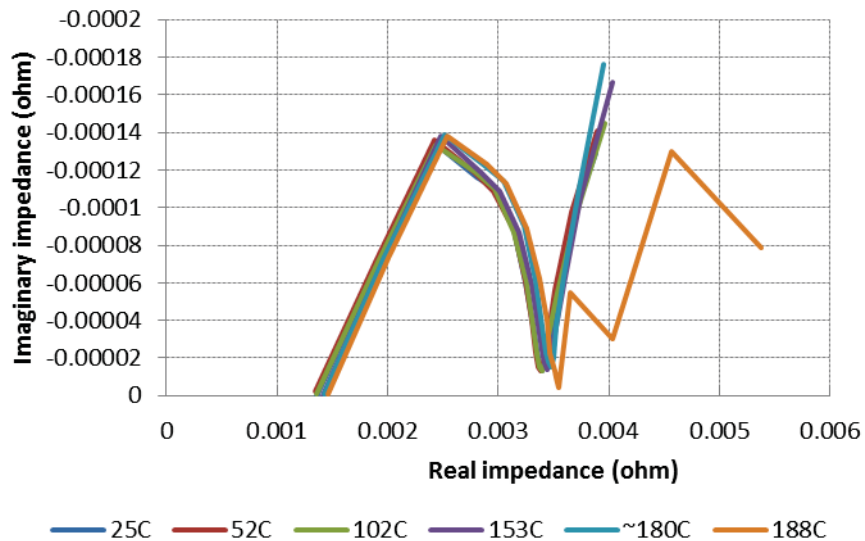


**Figure 29** Continuous impedance testing performed during 5 C/min thermal ramp with 20-second intervals between scans.

The impact of the heating rate on this technique was explored by applying 3 °C/min and 2 °C/min heating rates along with continuous impedance monitoring. This was done with 20 second intervals between scans, as the data in Figures 28 and 29 showed little apparent change as the scan rate was varied. The data collected at a 3 °C/min heating rate showed significantly more distinctness as the temperature was increased, as shown in Figure 30. The data shows little change up to 125 °C, however above that temperature the data begins to show a shift in the data similar to that observed for the step-by-step measurement method. There is then a large shift observed at 183 °C, just before the cell went into thermal runaway.

The data collected at 2 °C/min are shown in Figures 31 and 32, and has similar behavior. The low rate does allow for more distinct changes in the data at lower temperatures. The impedance curves remain relatively steady up to 47 °C, after which the minimum observed at  $\sim 0.0036 \Omega$  begins to shift to the left. This continues until a much larger shift is seen between 170 °C and 186 °C. Thermal runaway was observed in the cell shortly after the scan at 186 °C.

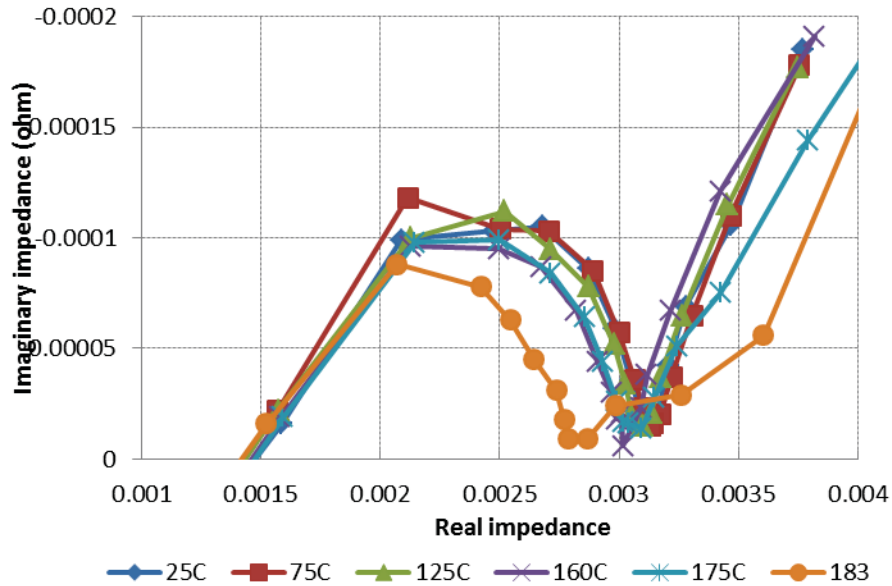


**Figure 30** Continuous impedance testing performed during 3 C/min thermal ramp with 20-second intervals between scans.

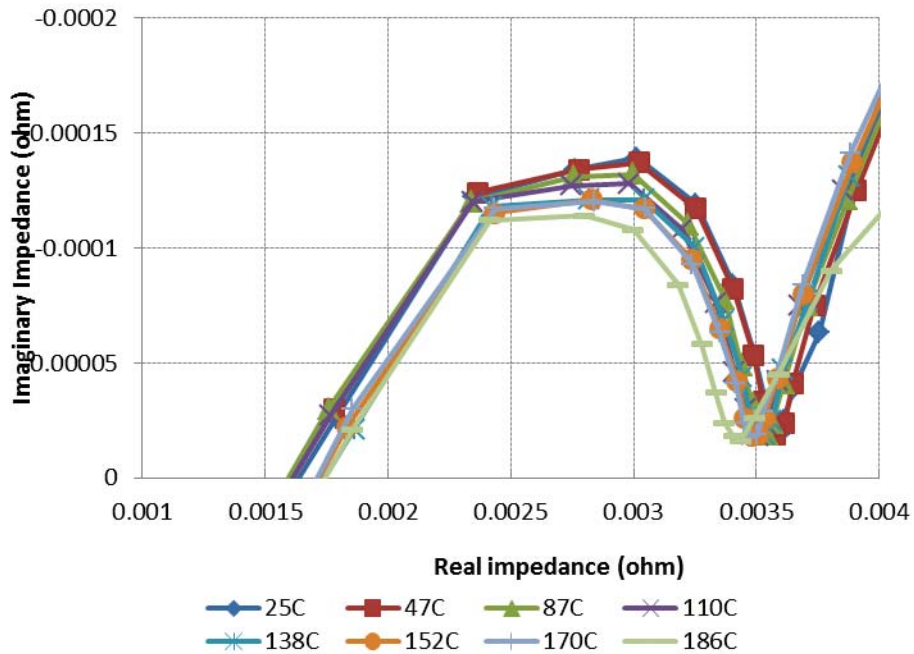


**Figure 31** Continuous impedance testing performed during 2 C/min thermal ramp with 20-second intervals between scans.

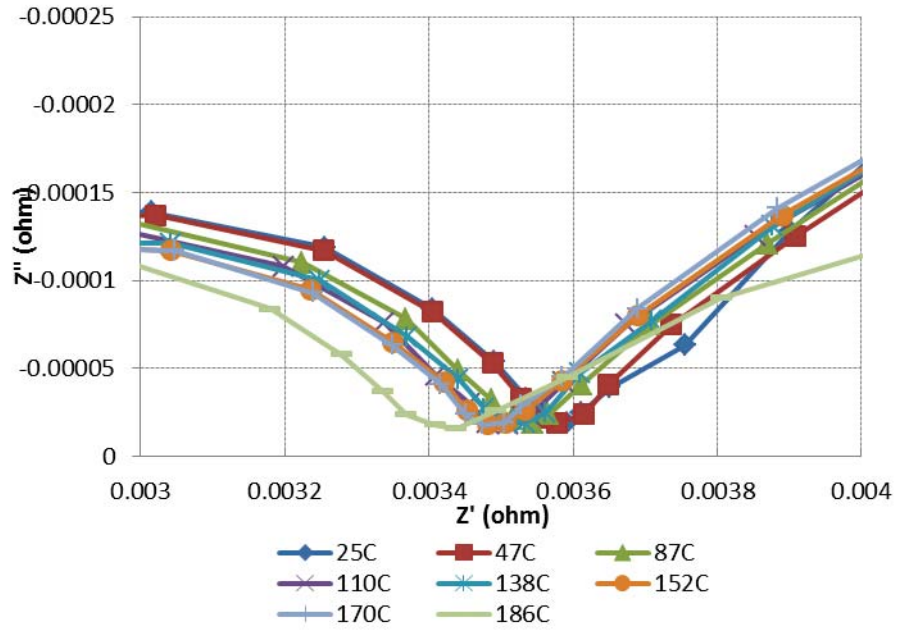


**Figure 32** Expanded view of Figure 31 above showing changes as the cell approaches runaway

## 4. CONCLUSIONS

Electrochemical impedance spectroscopy was demonstrated as an evaluation technique on 10 Ah LiCoO<sub>2</sub> lithium ion cells, as well as three-cell series and parallel strings constructed using the same cells. Specifically, EIS was used to look for changes in the data that could potentially be predictive of catastrophic failure when a battery is subjected to abusive conditions. The impedance measurement box developed at Idaho National Laboratory was also evaluated as a potential tool for real-time, on-board EIS evaluation of electrochemical cells and batteries.

Evaluation of single cells showed that for both overcharge and thermal abuse conditions, there was a measurable shift in the internal battery resistance as the abusive conditions increased. Overcharge testing showed small changes to the internal resistance at first, then as the overcharge increased to extreme levels, 180 to 200% SOC, the changes became much more dramatic. The behavior of the cells changed as well, showing near vertical lines on the impedance curve that are similar to the behavior of resistive elements. Plots of the internal resistance vs. the total state of charge show a measurable downturn in the internal resistance as the charge increases. This all is observed before evidence of cell heating occurs, potentially giving the ability to arrest overcharge before permanent damage is done to the cell.

Thermal ramp testing of single cells similarly showed significant shifts in the impedance data. As the cell was initially heated the internal resistance was observed to measurably decrease, however as the temperature approached hazardous levels the resistance began to increase significantly. The resistance can be observed to decrease as the cell heats from 25 °C to 100 °C, but then increases significantly from 100 °C to 125 °C, and again from 125 °C to 150 °C. The changes observed in single-cell testing both for the thermal ramp as well as overcharge abuse show shifts in the data that are large enough to be easily measured, even with single frequency impedance monitoring. Further, it should be noted that this chemistry showed a fairly resistive spectra, even at 50 °C, but this likely would not be true for all chemistries. In these cases complex EIS data may be necessary to provide an accurate measurement of behavior.

The need for complex impedance monitoring is demonstrated with the results of tests on three-cell strings. Overcharge testing of a single cell within a three-cell series string did not show the same dramatic changes in internal resistance. There was, however, an observable change in the charge transfer resistance as the level of overcharge was increased. Quantifying this change shows a marked drop as the total charge increases from 100% to 120%, followed more gradual decreases afterwards. Monitoring of this parameter could then be very effective at detecting even lower levels of overcharge within a system. A dramatic change in the behavior was also observed at very high levels of overcharge, with early onset of a Warburg tail and a larger drop in the charge transfer resistance. The early changes in charge transfer resistance in particular would likely be difficult to detect with single frequency impedance monitoring, and the change in total voltage of the series string at that stage is minimal. Complex impedance data allows for this change in behavior to be easily observed.

Thermal ramp testing of three-cell series strings show more well-defined changes as the level of abuse of a single cell within the string is increased. The impedance data remained relatively constant up to 100 °C, with only slight increases to the internal resistance observed. Above 100 °C, a significant increase in resistance is observed from 100 °C to 125 °C and again from 125 °C to 150 °C. While this occurs at temperatures high enough that a monitoring system would likely spot a potential problem, impedance diagnostics provide a redundant measurement to provide a more robust hazard mitigation strategy. This illustrates a means by which the presence of a localized unexpected temperature increase could be identified before a cell underwent thermal runaway.

Testing on parallel strings was limited to thermal ramp testing of a single cell, as overcharge cannot be applied to a single cell within a parallel configuration. These data show more subtle shifts in the impedance data as the temperature is increased. However, similar to the series strings the impedance data shows very little change up to 100 °C. At higher temperatures there is a shrinking of the semicircle in the Nyquist plot indicating a reduction in the charge transfer resistance. The presence of bulk changes above 100 °C in both the series and parallel configurations suggest that the bulk of the damage done to the cell occurs above 100 °C, but the nature of the changes in parallel configuration again show the benefit of complex impedance monitoring. Single frequency monitoring of the parallel string would show very little change except at very specific frequencies and even then would be a relatively small shift.

The IMB developed at INL was tested as well to evaluate its performance in analyzing behavior of single cells and three-cell parallel strings subjected to thermal abuse. Three-cell series strings were not evaluated as the unit available for testing carried a 5 V maximum. This testing also included use of the rapid-impedance measurements as a means to collect continuous scans on a cell or string as it approached failure. Testing of single cells gave data similar in behavior to that using the traditional tool. Little change was observed as the cell progressed from 25 °C to 100 °C. Above 100 °C the internal resistance was observed to increase fairly noticeably as the cell approached thermal runaway.

The three-cell string testing first attempted to re-create the data collected using the Solartron potentiostat. This was largely successful, with the IMB showing similar behavior. Both show little change up to 100 °C, followed by a shift in the charge transfer resistance as the temperature is increased above 100 °C towards runaway. The following tests evaluated data from the IMB as scans were applied continuously. These showed that the transient nature of thermally abusive tests with a fast heating rate can obscure in apparent data in multi-cell strings. Little change was observed when a single cell of a three-cell string was heated at 5 °C/min, but when the heating rate was reduced more significant shifts in the data became apparent.

#### **4.1 Technical challenges and future directions**

The primary technical challenges going forward will likely be the integration of impedance measurement into a battery system and analysis of measurements from larger, more complex systems. The data here shows that as the complexity of a battery system is increased, changes observed in the data become more subtle. This makes a good case for the use of complex impedance measurements, which can observe shifts in the data that may be obscured with single frequency impedance measurements, but still indicates the need for careful use and integration of

a monitoring system to properly observe changes. Follow on work currently planned will look at the use of impedance monitoring techniques on increasingly complex systems. Even then, there exists the possibility that any change to the data may become completely obscured if there is enough complexity in the pack being monitored. The data presented here does, however, provide evidence of measurable changes that occur even within increasingly complex systems.

Some practical concerns observed during testing are worth noting as well as rapid-impedance measurements are applied in the future. Some early lessons learned include:

- A small rest period is necessary between scans to limit noise within the measurement. Rest periods of up to 60 seconds were tested; a rest period of 20 seconds was found to be sufficient with little change in the data with longer rest periods.
  - Solution: A likely source of the need for a rest period is a memory issue within the control software. A newer generation of control software is under development for use with hardware capable of 50 V.
- Good separation of current cables and voltage signal cables should be maintained. This is particularly important when conducting abusive testing, as need for remote testing requires longer cables that increase the chance for inductive interference. This must be considered as well when onboard implementation of the hardware is being designed.
- Very transient battery systems can show little change in the impedance spectra. For example, in the case of the 5 °C/min thermal ramp, an impedance scan with a low frequency of 50 mHz will still take 20 seconds to complete, allowing for a shift of ~1.7 °C while the scan is being performed. Future work will need to include a careful analysis of the conditions where a battery may become unstable within a system to ensure that the tool is able to adequately detect any change in the complex impedance data.
  - Solution: Faster measurements (~ 1 second long) may be able to better measure changes in the charge transfer resistance.

## 5. REFERENCES

1. Abraham, D. P., Roth, E. P., Kostechi, R., McCarthy, K., MacLaren, S., & Doughty, D. H. (2006). Diagnostic examination of thermally abused high-power lithium-ion cells. *Journal of Power Sources*, 161(1), p. 648-657.
2. Doughty, D. H., Butler, P. C., Jungts, R. G., & Roth, E. P. (2002). Lithium battery thermal models. *Journal of Power Sources*, 110(2), p. 357-363.
3. Spotnitz, R. M., Weaver, J., Yeduvaka, G., Doughty, D. H., & Roth, E. P. (2007). Simulation of abuse tolerance of lithium-ion battery packs. *Journal of Power Sources*, 163(2), p. 1080-1086.
4. Jeevarajan, J. A. (2009). Limitations of internal protective devices in commercial low capacity cylindrical lithium-ion cells. Proceedings of the 3rd IAASS Conference Building a Safer Space Together, October, 21-23, 2008, Rome, Italy.
5. Jhu, C. Y., Wang, Y. W., Wen, C. Y., Chiang, C. C., & Shu, C. M. (2011). Self-reactive rating of thermal runaway hazards on 18650 lithium-ion batteries. *Journal of Thermal Analysis and Calorimetry*, 106(1), p. 159-163.
6. Lamb, J., & Orendorff, C. J. (2014). Evaluation of mechanical abuse techniques in lithium ion batteries. *Journal of Power Sources*, 247, p. 189-196.
7. Xu, F., He, H., Liu, Y., Dun, C., Ren, Y., Liu, Q., Wang, M., & Xie, J. (2012). Failure Investigation of LiFePO<sub>4</sub> Cells under Overcharge Conditions. *Journal of The Electrochemical Society*, 159(5), p. A678-A687.
8. Orendorff, C. J., Roth, E. P., & Nagasubramanian, G. (2011). Experimental triggers for internal short circuits in lithium-ion cells. *Journal of Power Sources*, 196(15), p. 6554-6558.
9. Kozlowski, J. D. (2001). A novel online measurement technique for AC impedance of batteries and other electrochemical systems. In Proceedings from the 16th Annual Battery Conference, January 9-21, 2001, Long Beach, CA.
10. Singh, P., Vinjamuri, R., Wang, X., & Reisner, D. (2006). Fuzzy logic modeling of EIS measurements on lithium-ion batteries. *Electrochimica Acta*, 51(8-9), p. 1673-1679.
11. Lasia, A. (2001). Comments on the article "An Electrochemical Impedance Measurement Technique Employing Fourier Transform" by J-S. Yoo & S-M. Park. *Analytical Chemistry*, 73(16), p. 4059-4059.
12. Yoo, J. S., & Park, S. M. (2000). An electrochemical impedance measurement technique employing Fourier transform. *Analytical Chemistry*, 72(9), p. 2035-2041.
13. Yoo, J. S., & and S.M. Park, S. M. (2001). Reply to comments on the article "An Electrochemical Impedance Measurement Techniques Employing Fourier Transform." *Analytical Chemistry*, 73(16), p. 4060-4061.
14. Kozlowski, J. D. (2003). Electrochemical cell prognostics using online impedance measurements and model-based data fusion techniques. In Proceedings from the IEEE Aerospace Conference, March 8-15 2003, Big Sky, MT.

15. Dahn, J. R., & Ehrlich, G. M. (2011). Lithium-Ion Batteries In T.B. Reddy, Ed., *Linden's Handbook of Batteries*. New York: McGraw Hill, p. 26.1-79.
16. Blanke, H., Bohlen, O., Buller, S., De Doncker, R. W., Fricke, B., Hammouche, A., ... Sauer, D. U. (2005). Impedance measurements on lead-acid batteries for state-of-charge, state-of-health and cranking capability prognosis in electric and hybrid electric vehicles. *Journal of Power Sources*, 144(2), p. 418-425.
17. Fleischer, C., Waag, W., Heyn, H-M., & Sauer, D. U. (2014). On-line adaptive battery impedance parameter and state estimation considering physical principles in reduced order equivalent circuit battery models, Part 1. Requirements, critical review of methods and modeling. *Journal of Power Sources*, 260(0), p. 276-291.
18. Fleischer, C., Waag, W., Heyn, H-M., & Sauer, D. U. (2014). On-line adaptive battery impedance parameter and state estimation considering physical principles in reduced order equivalent circuit battery models part 2. Parameter and state estimation. *Journal of Power Sources*, 262(0), p. 457-482.
19. Srinivasan, R., Carkhuff, B. G., Butler, M. E. & Baisden, A. C. (2011). Instantaneous measurement of the internal temperature in lithium-ion rechargeable cells. *Electrochimica Acta*, 56(17), p. 6198-6204.
20. Schmidt, J. P., Arnold, A., Loges, A., Werner, D., Wetzels, T., & Ivers-Tiffée, E. (2013). Measurement of the internal cell temperature via impedance: Evaluation and application of a new method. *Journal of Power Sources*, 243, p. 110-117.
21. Love, C. T., & Swider-Lyons, K. (2012). Impedance Diagnostic for Overcharged Lithium-Ion Batteries. *Electrochemical and Solid-State Letters*, 15(4), p. A53-A56.
22. Christophersen, J. P., Morrison, J. L., Rose, D. M., Morrison, W. H., & Motloch, C. G. (2012). Crosstalk compensation for a rapid, higher-resolution impedance spectrum measurement. In *Proceedings of the 2012 IEEE Aerospace Conference*, March 3-10, 2012, Big Sky, MT, p. 16.
23. Ramamurthy, A., Notani, S. & Bhattacharya, S. Advanced lithium ion battery modeling and power stage integration technique. In *Proceedings of the 2010 IEEE Energy Conversion Congress and Exposition*, September 12-16, 2010, Atlanta, p. 1485-1492.
24. Morrison, J.L., Christophersen, J. P., Morrison, W. H. (2014). Universal auto-calibration for a rapid battery impedance spectrum measurement device. In *Proceedings of the 2014 IEEE Aerospace Conference*, March 1-8, 2014, Big Sky, MT, p. 8.
25. Doughty, D. H., & Crafts, C. C. (2006). *FreedomCAR Electrical Energy Storage System Abuse Test Manual for Electric and Hybrid Electric Vehicle Applications*. Albuquerque, NM: Sandia National Laboratories.

DOT HS 812 249  
March 2016



U.S. Department  
of Transportation  
**National Highway  
Traffic Safety  
Administration**

